Major geomagnetic storms ($Dst \leq -100$ nT) generated by corotating interaction regions

I. G. Richardson[1, 2], D. F. Webb[3], J. Zhang[4], D. B. Berdichevsky[1, 5], D. A. Biesecker[6], J. C. Kasper[7], R. Kataoka[1], J. T. Steinberg[8], B. J. Thompson[1], C.-C. Wu[9], and A. N. Zhukov[10, 11]

Abstract.
Seventy-nine major geomagnetic storms (minimum $Dst \leq -100$ nT) observed in 1996 to 2004 were the focus of a "Living with a Star" Coordinated Data-Analysis Workshop (CDAW) in March, 2005. In 9 cases, the storm driver appears to have been purely a corotating interaction region (CIR) without any contribution from coronal mass ejection-related material (interplanetary coronal mass ejections, ICMEs). These storms were generated by structures within CIRs located both before and/or after the stream interface that included persistently southward magnetic fields for intervals of several hours. We compare their geomagnetic effects with those of 159 CIRs observed during 1996 – 2005. The major storms form the extreme tail of a continuous distribution of CIR geoeffectiveness which peaks at $Dst \sim -40$ nT but is subject to a prominent seasonal variation of ~ 40 nT which is ordered by the spring and fall equinoxes and the solar wind magnetic field direction towards or away from the Sun. The *O'Brien and McPherron* [2000] equations, which estimate Dst by integrating the incident solar wind electric field and incorporating a ring current loss term, largely account for the variation in storm size. They tend to underestimate the size of the larger CIR-associated storms by $Dst \sim 20$ nT. This suggests that injection into the ring current may be more efficient than expected in such storms. Four of the nine major storms in 1996 – 2004 occurred during a period of less than three solar rotations in September – November, 2002, also the time of maximum mean IMF and solar magnetic field intensity during the current solar cycle. The maximum CIR-storm strength found in our sample of events, plus additional 23 probable CIR-associated $Dst \leq -100$ nT storms in 1972 – 1995, is ($Dst = -161$ nT). This is consistent with the maximum storm strength ($Dst \sim -180$ nT) expected from the *O'Brien and McPherron* equations for the typical range of solar wind electric fields associated with CIRs. This suggests that CIRs alone are unlikely to generate geomagnetic storms that exceed these levels.

1. Introduction

Major geomagnetic storms are among the most important space weather phenomena. The 79 storms occuring during 1996 to 2004 with minimum $Dst \leq -100$ nT were the focus of a "Living with a Star" Coordinated Data-Analysis Workshop (CDAW) held at George Mason University, Fairfax, VA, in March, 2005. A major aim of the workshop was to identify the interplanetary drivers of these storms, and where possible, their solar counterparts. Consistent with previous studies [e.g., *Gosling et al.*, 1991; *Tsurutani and Gonzalez*, 1997; *Richardson et al.*, 2001; *Zhang et al.*, 2003] the majority of these storms were found to be driven by interplanetary coronal mass ejections (ICMEs) and/or the related upstream sheaths, or multiple structures of these types. The remaining events generally involved a corotating interaction region (CIR) formed ahead of a high-speed stream emanating from a coronal hole. In some 4 cases, the CIR interacted with a preceding ICME, and compression of southward magnetic fields in the ICME intensified the geoeffectiveness. Similar events have been reported by *Zhao* [1992], *Cane and Richardson* [1997], *Fenrich and Luhmann* [1998] and *Crooker* [2000]. In another 9 cases, the CIR alone was responsible for driving the storm, with little or no evidence of ICME-like structures being involved, and no plausible association with earthward-directed coronal mass ejections (CMEs) observed by the SOHO/LASCO coronagraphs. This observation is somewhat surprising given that some previous studies [e.g., *Gonzalez et al.*, 1999, and references therein] that have concluded that CIRs never generate storms with $Dst < -100$ nT. Three examples in 1994 were identified by *Watari* [1997], however, and an additional event (October 23, 1996) was reported by *Zhang et al.* [2003].

In Section 2, we describe solar wind observations associated with these 9 CIR-associated storms. In Section 3, we

[1]NASA Goddard Space Flight Center, Greenbelt, MD.
[2]Department of Astronomy, University of Maryland, College Park.
[3]Boston College, Institute for Scientific Research, Chestnut Hill, MA.
[4]George Mason University, Fairfax, VA.
[5]L-3 Government Services Inc.
[6]NOAA/Space Environment Center, Boulder, CO.
[7]MIT Center for Space Research, Cambridge, MA.
[8]Los Alamos National Laboratory, Los Alamos, NM.
[9]CSPAR/University of Alabama in Huntsville, AL.
[10]Royal Observatory of Belgium, Brussels, Belgium.
[11]Skobeltsyn Institute of Nuclear Physics, Moscow State University, Moscow, Russia.

0148-0227/06/$9.00

discuss these observations in the context of a sample of 159 CIRs during cycle 23, and examine the relationship between CIR/stream properties and the storms that they generate.

2. Observations

The nine CIR-associated $Dst \leq -100$ nT storms in 1996 – 2004 are listed in Table 1, where the first two columns give the time of the storm peak and minimum Dst. We also show the minimum value of the pressure corrected Dst index, $Dst^* = Dst - 7.26P_d^{0.5} + 11$ nT, where P_d is the solar wind dynamic pressure in nPascals [*O'Brien and McPherron*, 2000]. For these storms, minimum Dst^* and Dst differ by ≤ 7 nT. Evidently, the storms were not distributed evenly during this period, which extends from sunspot minimum through sunspot maximum for cycle 23 (in 2000) and into the declining phase of this cycle. There were only two events during the ascending phase of the cycle, and no events during a $\sim$ 4-year interval around sunspot maximum. The remaining events occurred during the declining phase. A caveat should be added that the 2003 and later events were identified using the provisional Dst index and may be revised when the final index becomes available.

It is well established that the dawn-dusk ($-y$) component of the solar wind electric field ($\mathbf{E} = -\mathbf{V} \times \mathbf{B}$) is an important driver of geomagnetic activity [e.g., *Dungey*, 1961; *Perrault and Akasofu*, 1978; *Tsurutani and Gonzalez*, 1997, and references therein], including activity associated with CIRs [*Burlaga and Lepping*, 1977]. Hence, we have examined solar wind plasma and magnetic field observations associated with each of these storms to infer the characteristics of their drivers. For those in 1998 – 2004, 64-s plasma/field observations from the ACE spacecraft were used; similar 92-s WIND data were used for earlier events or when there were ACE plasma data gaps. Relevant parameters for these events are shown in Figures 1 to 4. For each event, the top black graph shows the hourly Dst index. Other graphs show the magnetic field intensity and z- (north-south) component, the y-component of the solar wind electric field ($E_y = -V_x B_z$) in Geocentric Solar Magnetospheric (GSM) coordinates, the azimuthal magnetic field angle (ϕ_B, where 0^o = directed sunward and 90^o is directed to the east), plasma proton temperature (T_p), density (n), bulk speed (V), and flow angle (ϕ_{sw}), and the hourly-averaged ratio of solar wind oxygen ions with charges 7 and 6 (O^7/O^6) from the ACE/SWICS instrument, if available. The plasma and field data illustrated are generally from ACE. However, WIND data are used if they are more complete than the ACE data. If WIND data are displayed, we do still show E_y based on ACE data – inspection of variations in E_y (ACE) and B_z (WIND) verifies that essentially similar structures were observed at both spacecraft (after allowing for the few tens of minutes propagation delay from ACE to WIND) and serves to "link" the ACE composition data with the WIND data.

To illustrate some of the features of a representative event, consider the storm of March 10, 1998, shown in Figure 1. We conclude that this storm was associated with a CIR based on its association with a region of compressed plasma, indicated by enhanced plasma densities (reaching $\sim$ 60 /cc) and magnetic field intensities (reaching $\sim$ 24 nT), lying at the leading edge of a high-speed stream – note that the solar wind speed increases from $\sim$ 300 km/s at the start of the plot to nearly 600 km/s during the second half of March 10. Typical plasma and magnetic field signatures of interaction regions and high-speed streams at $\sim$ 1 AU are discussed for example by *Belcher and Davis* [1971] and *Schwenn* [1990]. The unusually high densities are associated with the heliospheric plasma sheet [e.g., *Winterhalter et al.*, 1994; *Bavassano et al.*, 1997; *Crooker et al.*, 2004a, and references therein] encompassing the heliospheric current sheet that was crossed at $\sim$ 02, 05 and 09 UT on March 10. WIND/3DP and ACE/SWEPAM solar wind suprathermal electron pitch-angle distributions (not illustrated here) show reversals of the anti-solar heat flux relative to the magnetic field direction at these times, suggesting that these were true current sheet crossings rather than current sheets associated with folded field lines. See e.g., *Kahler and Lin* [1995] and *Crooker et al.* [2004a, b], and references therein, for a discussion of using solar wind electron flows to identify true heliospheric current sheet crossings.

The stream interface, a narrow structure (often a discontinuity) separating accelerated slow solar wind and decelerated fast stream plasmas, is a prominent feature of CIRs [e.g., *Burlaga*, 1974; *Gosling et al.*, 1978; *Schwenn*, 1990; *Forsyth and Marsch*, 1999, and references therein]. The interface is typically indicated by a relatively abrupt depression in the plasma density, increases in V and T_p, and the solar wind flow direction ϕ_{sw} changing from $> 0^o$ to $< 0^o$. We suggest that the interface was crossed at $\sim$ 12 UT on March 10, as indicated by the vertical green line in Figure 1. The decrease in the solar wind O^7/O^6 ratio at this time is consistent with this interpretation [*Wimmer-Schweingruber et al.*, 1997]. The overlaid (red) line gives the (V-dependent) O^7/O^6 ratio expected for "normal" (non-ICME) solar wind [*Richardson and Cane*, 2004], and suggests that the observed O^7/O^6 ratios are consistent with normal solar wind. In particular, there is no clear evidence of ICME-related material, which typically has higher than expected O^7/O^6 ratios [*Richardson and Cane*, 2004, and references therein]. The absence of enhanced iron charge states observed by ACE/SWICS [e.g., *Lepri et al.*, 2001] supports this conclusion, as does the absence of abnormally low proton temperatures which can be indicative of ICME material [e.g., *Richardson and Cane*, 1995] - the expected temperature is overlaid on the T_p panel in Figure 1. Rather, as is typical of CIRs, T_p was slightly enhanced above normal values, presumably as a result of compressional heating resulting from the stream-stream interaction.

The driver of the March 10, 1998 storm was a $\sim$ 6–hour interval of nearly persistent southward magnetic field that reached $\sim$ 17 nT during the trailing half of the CIR ("F' region" of *Belcher and Davis* [1971]). The transverse solar wind electric field reached ~ -9 mV/m at this time. Figure 5 summarizes the z-components of the magnetic field and solar wind velocity during the structures that drive this and the other storms in Table 1. For the March 10, 1998 storm, correlated variations in B_z and V_z indicate the presence of Alfvén waves moving out from the Sun. Such waves are a common feature of CIRs and high-speed streams [e.g., *Belcher and Davis*, 1971; *Smith et al.*, 1995] and may be amplified when they propagate into the CIR [*Tsurutani et al.*, 1995a]. In particular, the interval of predominantly southward field responsible for this storm commenced with large-amplitude Alfvén waves at $\sim$ 14 UT. Nevertheless, there may have been a non-Alfvénic component since the persistent southward field, extending to $\sim$ 17 UT has no apparent counterpart in V_z. The origin of this strong southward field is unclear. As noted above, there are no clear signatures suggesting the presence of an ICME. In addition, the last halo/partial halo CME observed by SOHO/LASCO was on February 28 according to the LASCO catalogue (http://cdaw.gsfc.nasa.gov/CME_list/), far too early to be involved in this storm. A further argument against an ICME structure being involved in the production of this storm is that the solar wind that drives the storm is on the high-speed, coronal hole flow side of the interface.

Crooker et al. [2004a, b] suggest that fields that deviate from the expected Parker spiral direction in longitude and latitude can arise in looped structures formed by interchange reconnection at the heliospheric current sheet. However, there is little evidence of such structures on March 10 since, as noted above the magnetic and energetic electron polarity changes occur together suggesting the presence only of true current sheet crossings. Furthermore, the heliospheric plasma sheet was on the opposite side of the stream interface from the geoeffective structure. Hence, it seems unlikely that the storm driver is related to the heliospheric plasma sheet.

The likely solar source of the stream was an equatorward extension of the southern polar coronal hole indicated by the arrow near central meridian in the SOHO EIT Fe XV observation for March 7, 1998 shown in Figure 6. By March 10, this coronal hole would have rotated to $\sim 40^o$ west, consistent with the location of footpoints of field lines in the high-speed stream observed at Earth. The sunward magnetic field direction in the high-speed stream is consistent with the direction of the field in the southern polar coronal hole prior to the maximum of Cycle 23.

Two other storms generated by intervals of southward field extending from the vicinity of the stream interface to the CIR trailing edge are shown in Figure 1. The storm of September 4, 2002 ($Dst = -109$ nT) was driven by a similar $\sim$ 4 hour period of $<=$ 20 nT southward field and transverse electric fields ~ -7 mV/m in the vicinity of, and following, the stream interface, though with less evidence of Alfvénic fluctuations (Figure 5). The suggested interface, bounded by the two vertical green lines in Figure 1, is a structure encompassing the start of the increase in T_p and decrease in O^7/O^6 to the deflection of the flow angle through the radial direction and an abrupt decrease in density. The proximity of the strongest southward fields to the interface suggests that the stream-stream interaction may have been involved in the production of the out-of-the-ecliptic fields. Ahead of the stream interface, the smooth rotation in magnetic field direction on September 3 (which includes a slow sector boundary) and enhanced field intensity resemble the features of the subset of ICMEs known as "magnetic clouds" [*Klein and Burlaga*, 1982]. Furthermore, bidirectional suprathermal electron flows, often a signature of ICMEs [e.g., *Gosling*, 1990] were present, and the Genesis spacecraft on-board solar wind algorithm [*Neugebauer et al.*, 2003] classified the interval from $\sim$ 04 to 16 UT as likely ICME material. Thus, it is possible that ICME material was present. On the other hand, enhanced O^7/O^6 and low T_p are absent, and this structure is not identified by the automated magnetic cloud identification scheme of *Lepping et al.* [2005]. In any case, this structure had a northward-directed magnetic field and did not contribute to the geomagnetic storm. The last preceding, catalogued LASCO halo/partial halo CME was $\sim$ 4 days earlier at 0306 UT on August 30 but the high CME speed (1111 km/s) and strong asymmetry towards the west suggest that this CME was unlikely to be associated with the structures related to the September 4 storm. A weak inhomogeneous outflow at a wide range of position angles starting at 1506 UT on August 29 that is not included in the CME catalogue might be an alternative source candidate. A reverse shock was present at the CIR trailing edge (red vertical line) but clearly had no role in the storm. The outward magnetic field direction in the high-speed stream is consistent with an association with the southern coronal hole indicated in the SOHO/EIT observations for August 30, 2002 (after the solar polar field reversal at solar maximum) in Figure 6.

The third storm in Figure 1 driven by the trailing half of a CIR, October 23, 1996, reached $Dst = -105$ nT, and was generated by a 7-hour interval of nearly persistent, southward magnetic fields that reached $\sim$ 12 nT, together with transverse electric fields of $\sim$ 7 mV/m. Figure 5 suggests that these southward fields were associated with Alfvén waves. The available WIND data show little evidence of ICME-like signatures, such as low T_p. Another point to note is that the heliospheric plasma sheet was not crossed in this CIR. A partial halo CME with a speed of 480 km/s was observed by LASCO at 1717 UT on October 19. Although the $\sim$ 3-day interval between the CME and storm onset is reasonably consistent with the CME speed, EIT and Yokhoh STX observations show that the related activity was in the south-east quadrant of the solar disk, outside the trailing-edge of the coronal hole that gave rise to this CIR, indicated in the observations for October 20, 1996 in Figure 6. Thus, it is unlikely that this CME would have been detected at Earth at the leading-edge of the stream.

A second group of three storms were driven by intervals of southward fields that largely preceded the stream interface (S' region). These storms are shown in Figure 2, in order of decreasing time interval between the storm peak and interface crossing.

The storm on February 11, 2004 ($Dst = -109$ nT) was caused by an $\sim$ 9 hour period of southward magnetic fields reaching $\sim$ 15 nT and transverse electric fields ~ -6 mV/m. Recovery commenced when the field turned northward $\sim$ 8 hours before the interface. While the enhanced southward followed by northward fields might indicate the presence of a magnetic cloud-like structure, there is no evidence of unusually high ion charge states (cf., O^7/O^6) or abnormally low T_p, and this region is not selected by the automatic cloud detection scheme. Also, no LASCO halo/partial halo CMEs were reported after January 26. Figure 5 suggests that the solar wind on February 11, 2004 was dominated by Alfvénic fluctuations. In particular, the larger-scale north-south field variations that influence geoeffectiveness are largely reflected by V_z. The elevated densities in the southward field region together with crossings of the heliospheric current sheet suggest that this region is associated with the heliospheric plasma sheet. However, ACE/SWEPAM electron distributions suggest that the only true sector boundary crossing occurred near the beginning of February 11. The origin of the high-speed stream is a large, low latitude coronal hole with a thin extension to the north pole (see observations for February 10, 2004 in Figure 6). The sunward magnetic field direction is consistent with the inward field direction above the north pole.

The driver of the $Dst = -115$ nT storm on October 7, 2002 was $\sim$ 1-day period of modest ($<$ 10 nT) southward field, and $E_y >\sim -3$ mV/m ahead of the interface. Variations in B_z are largely associated with Alfvén waves (Figure 5), and there are no ICME-like signatures. Dst was already at ~ -50 nT before the CIR arrived. Thus, it is likely that this CIR with modest plasma/field signatures would not have produced a major storm without this ongoing "pre-conditioning" activity. The probable stream source is the equatorward southern coronal hole extension indicated in the observations for October 4, 2002 in Figure 6.

The storm of October 14, 2002 ($Dst = -100$ nT) was driven by a $\sim$ 10 hour interval of nearly persistent southward-directed field, associated with the heliospheric plasma sheet, that reached $\sim$ 16 nT, was accompanied by transverse electric fields of $\sim$ 5 mV/m, and terminated at the stream interface. Both ACE/SWEPAM and Genesis show evidence of bidirectional suprathermal electron distributions within this structure, suggesting the possible presence of a looped field structure that might be indicative of an ICME. On the other hand, there are no clear signatures of ICME-like material in T_p and O^7/O^6. There were partial halo CMEs on October 9, but frontside activity was at low levels, suggesting that they were probably backsided. The high-speed stream most likely emerged from the coronal hole indicated in the EIT observations for October 12, 2002 in Figure 6.

Two storms contain components driven by structures both before and after the stream interface (Figure 3). That on November 21, 2002 had two minima ($Dst = -87$ nT and

−128 nT). The region of southward magnetic field forming the driver of the first component shows ϕ_B slowly reversing from sunward to outward and then back to sunward. ACE/SWEPAM (and WIND-3DP) electrons suggest that these are field folds or loops in the vicinity of the heliospheric plasma sheet and that the true sector boundary crossing was not until $\sim$ 05 UT on November 21, close to the time of the interface crossing. Large amplitude Alfvén waves were also present (Figure 5). The forward shock at the CIR leading edge evidently plays no role in storm generation. The second *Dst* minimum is associated with amplified Alfvén waves in the trailing half of the CIR (Figure 5) that are geoeffective because they have predominantly southward, and few strong northward, field components that reach $\sim$ 20 nT, and produce transverse electric fields reaching ~ -12 mV/m. This second storm component does not build on the first component since activity declines during the intervening period due to a nearly 40 nT field enhancement with strong northward fields centered on a sector boundary crossing. Though this structure resembles a magnetic cloud/flux-rope with a northward-directed axis, there is little supporting evidence in T_p or O^7/O^6. A halo CME was observed by LASCO at 0712 UT on November 16, but the high speed (1185 km/s) compared with the low implied transit speed (420 km/s), asymmetry, and probable backsided source (G. Lawrence, preliminary LASCO CME report) suggest that it was not related to interplanetary structures associated with this storm. The high-speed stream most likely originated in an equatorward extension of the southern coronal hole indicated in observations for November 19, 2002 in Figure 6.

The storm with a peak on July 12, 2003 also had two components, with local minima on July 11 ($Dst = -74$ nT) and July 12 (-118 nT). The first component was driven by a $\sim$ 16 hour interval of persistent southward field extending through the leading half of the CIR up to and including the stream interface, reaching values of $\sim$ 12 nT ($E_y \sim -5$ mV/m). This structure might have been ICME-related based on evidence of slightly depressed T_p and elevated oxygen charge states (Figure 3), and an absence of large-amplitude Alfvén waves (Figure 5). In addition, the Genesis algorithm identified possible ICME material between $\sim$ 02 UT and the stream interface on July 11. There is no CME candidate associated with the structures on July 10-11: The last reported LASCO halo/partial halo CME (with a speed of 751 km/s), on July 4, was too early and highly asymmetric, directed to the east. The second phase of the storm was associated with variable but predominantly southward fields in the trailing half of the CIR that included Alfvén waves and reached $\sim$ 16 nT ($E_y \sim -9$ mV/m). The source of this high-speed stream was the low-latitude coronal hole with a narrow extension from the north polar hole indicated in the observations for July 9, 2003 in Figure 6.

The final storm to be considered (July 16, 2003; Figure 4) differs from the other storms in Table 1 in that it was apparently produced by an interaction region formed between two high-speed ($\sim$ 600 km/s) coronal hole streams – note the intervals of enhanced field intensity and plasma density, a possible interface at $\sim$ 1330 UT on July 16, and a reverse shock at the trailing edge of the CIR. The storm was caused by the $\sim$ 8 hour duration region of southward magnetic field ahead of the interface. There are no compelling ICME-like signatures except for a slight enhancement over expected values of O^7/O^6, and this might indicate instead slower plasma (with higher charge states) that has been accelerated in this unusual stream configuration. Also, Genesis identified fast stream, non-CME, solar wind throughout the interval in Figure 4. The north-south field variations are dominated by Alfvén waves (Figure 5). EIT observations for July 15, 2003 (Figure 6) show a large coronal hole extending from the south-east solar limb to the north polar coronal hole, with a branch towards the west limb. Thus, it is possible that the interaction is between flows emerging from different regions of this coronal hole. The sunward-directed magnetic fields before and after the interaction region would be consistent with this scenario and with the polarity of the northern polar coronal hole. No halo/partial halo LASCO CMEs are reported after the July 4 CME mentioned in the preceding paragraph.

3. Discussion

The common factor generating the storms in Table 1 is the presence of structures within CIRs in which the magnetic field is enhanced, presumably because of compression resulting from the interaction and, most importantly, remains predominantly southward-directed for several hours, allowing time for the storm to develop. Southward magnetic fields of at least 10 nT, and transverse electric fields of < -5 mV/m are typically required. These geoeffective structures occur equally frequently before and after the stream interface, and if present both before and after the interface, may lead to a storm with two components. A role for transients in larger CIR-associated storms has been advocated by, for example, *Crooker and Cliver* [1994], *McAllister and Crooker* [1997], *McAllister et al.* [1998], and *Crooker et al.* [2004a, b], but this view is not strongly supported by the events discussed here. The geoeffective structures generally do not have conspicuous ICME-like signatures, in particular low T_p and high ion charge states (e.g., enhanced O^7/O^6), suggesting that they are unlikely to be related to CMEs. The driver of the first phase of the July 12, 2003 storm may be an exception. There are no Earthward-directed halo CMEs observed by the SOHO/LASCO coronagraphs that may be plausible associated with these storms, although we note that ICMEs can be observed at Earth in the absence of halo CMEs detectable by LASCO [e.g., *Cane and Richardson*, 2003]. Suprathermal solar wind electrons suggest that in several cases, the storm driving regions are associated with folded or looped fields in the heliospheric plasma sheet. Thus, it is possible that they involve transient structures, such as envisaged by *Crooker et al.* [2004a] to be formed by interchange reconnection. Such structures are unlikely to have typical ICME signatures since they form higher in the corona. Correlations between the north-south solar wind velocity and magnetic field components in most of these structures suggest that large amplitude Alfvén waves are present and can contribute to, if not provide the dominant source of, the southward fields.

The importance of the time variation of B_s (and E_y) in determining storm size is illustrated by the CIR on January 27, 2000 (Figure 7). Although southward fields reach $\sim$ 25 nT, these are brief and interspersed with northward fields that reach similar intensities such that the storm only reaches $Dst = -41$ nT. Note also the initial large positive excursion in *Dst* (reaching +46 nT, or +20 nT if pressure-corrected) caused by compression of the magnetosphere at the time of the exceptionally large densities in the CIR. Figure 7 illustrates that a reasonably high-speed stream ($\sim$ 750 km/s with a change in speed of $\sim$ 400 km/s) including a well-developed CIR at the leading edge and a sector boundary crossing may not necessarily lead to a major geomagnetic storm.

To quantify this discussion of the conditions that generate CIR-associated storms, we have used the *O'Brien and McPherron* [2000] (OM) equations that relate the pressure-corrected *Dst* index to the solar wind driver given by VB_s, where VB_s is the rectified value of VB_z that is positive when B_z is southward and zero when B_z is northward. These equations are:

$$\frac{d}{dt}Dst^* = Q(VB_s) - \frac{Dst^*}{\tau(VB_s)}, \tag{1}$$

$$Q(VB_s) = \begin{cases} \alpha(VB_s - E_c) & VB_s > E_c, \\ 0 & VB_s \leq E_c, \end{cases} \quad (2)$$

$$\tau(VB_s) = \tau_\infty \exp(\frac{V_o}{V_q + VB_s}). \quad (3)$$

The rate of change of Dst^* is assumed to be proportional to VB_s, Q representing injection into the ring current, less a loss term represented by the recovery time τ that depends on the strength of the ring current and is assumed to be proportional to Dst. *O'Brien and McPherron* [2000] estimate that $\alpha = -4.4$ nT m(mV h)$^{-1}$, $E_c = 0.5$ mV/m, $\tau_\infty = 2.4$ hours, $V_o = 9.7$ mV/m, and $V_q = 4.7$ mV/m. Note that the recovery time τ depends on the incident VB_s and ranges from a maximum of 18.9 hours (for $VB_s = 0$) to $\sim$ 4–5 hours for typical values of VB_s ($\sim$ 5–10 mV/m) associated with the CIR events discussed above.

In Figures 1–4, we have plotted in the upper panels the time variation of Dst^* "predicted" by the OM equations for each of the CIR-associated storms. The calculation uses the ACE 64-s or WIND 92-s GSM V_x and B_z as input, and starts well ahead of each event so that the solution has stabilized by the time of the storm. Note that we compare in the figures the predicted Dst^* with Dst rather than Dst^*. Although the difference between Dst and Dst^* can be significant within the dense plasma inside CIRs, it is typically only a few nT at storm maximum (cf., Table 1). Overall, the observed variations in Dst are replicated fairly successfully with the exception of some details, such as the faster recovery between the components of the November, 2002 storm, suggesting that the physical assumptions of the OM equations together with the observed interplanetary conditions can largely account for the generation of these major storms.

To place the storms in Table 1 in context, we have examined the geomagnetic activity (as measured by Dst) for a total of 159 CIRs/high-speed streams in the near-Earth solar wind during 1996 – early 2005 that did not involve any ICMEs (as identified for example by *Cane and Richardson* [2003]). This sample includes the vast majority of such CIRs that encountered Earth during this period, including those associated with the major storms discussed in this paper. (A few streams were excluded, for example, at times of ongoing ICME-associated storms). The top panel of Figure 8 shows the minimum Dst in each of these streams (typically associated with the passage of the CIR) plotted as a function of time (events in Figure 8 prior to 1996 will be discussed below). It is clear that the streams with $Dst \leq -100$ nT are exceptional, and the majority are associated with weaker storm conditions. Figure 9 shows a histogram of the number of events vs. minimum Dst. The distribution peaks at $Dst \sim -40$ nT, with a tail extending to lower Dst values. In this sample of events, $\sim$ 6% generate storms with $Dst \leq -100$ nT, the strongest storm having $Dst = -128$ nT. The mean Dst is -46 nT. For comparison, Figure 9 also shows the distribution of minimum Dst for 281 ICME-associated storms in 1996–2005, updated from the list of *Cane and Richardson* [2003]. Interestingly, the distribution for ICMEs also peaks at ~ -40 nT, suggesting that the most probable (Dst) activity is similar for CIRs and ICMEs. However, ICMEs clearly have a more extended tail to low Dst values reaching (in this sample of events) nearly -500 nT and resulting in a lower mean (-76 nT). There are relatively fewer CIRs than ICMEs associated with Dst near 0 nT, suggesting that CIRs are rarely associated with geomagnetically quiet conditions. A probable explanation is that the combination of large-amplitude Alfvén waves, which are likely to include some southward field components, and high-speed flows mean that most CIRs/high-speed streams are likely to be geoeffective to some extent. On the other hand, ICMEs and sheath plasma can occasionally include persistent northward fields that are not geoeffective. Again we caution that storm sizes for events in 2003 and later may be revised when final Dst values become available.

The storms in Table 1 show a tendency to be clustered around the March and September equinoxes, suggestive of a seasonal effect. Furthermore, the structures driving the storm have sunward-directed fields (-ve in Table 1, column 5) in the two cases near the spring equinox, and anti-solar fields (+ve in Table 1, column 5) in those events near the fall equinox. Such a pattern is consistent with the expectations of the *Russell and McPherron* [1973] effect, to which other factors also contribute [e.g., *Cliver et al.*, 2000; *O'Brien and McPherron*, 2002]. The seasonal influence in the geoeffectiveness of our sample of CIRs is demonstrated further in Figure 10, which shows minimum Dst for these CIRs as a function of month of the year, divided into events in which the magnetic field direction in the structure driving the activity is towards or away from the Sun. Mean values of Dst for events in each month are also indicated. It is evident that overall activity levels are higher during the months around the fall solstice for anti-solar fields, and higher around the spring solstice for sunward fields. The difference in average Dst between favored and unfavored field directions is as much as $\sim$ 40 nT which is a significant fraction of the -100 nT major storm threshold used to identify the workshop events. Thus, we conclude that the seasonal effect is an important factor in enhancing the geoeffectiveness of structures associated with CIRs/streams with favored field directions and hence in producing major CIR-associated storms. The only major storms which deviate from this seasonal pattern are those of July, 2003 which occur away from both solstices.

We have calculated the predicted storm size from the OM equations for each event (if essentially complete plasma and field data are available) and compare these results in Figure 11 with the observed minimum Dst^* and Dst. The predicted storm sizes (for 154 events) are highly correlated both with Dst^* ($cc = 0.862$) and Dst ($cc = 0.872$). Note though that the observed geomagnetic activity during the largest CIR-associated storms (as measured by Dst or Dst^*) tends to exceed predicted levels by ~ -20 nT. In particular, only one storm is predicted to exceed -100 nT. A possible interpretation is that the ring current injection efficiency for CIR-associated activity, represented by Q, is higher than inferred by OM. In fact, *Miyoshi and Kataoka* [2005] conclude that Alfvén waves associated with CIRs result in repeated injections from the plasma sheet into the ring current which may increase the overall ring current injection efficiency. Figure 10 shows the storm sizes predicted by the OM equations as a function of month of year. These largely reproduce the observed seasonal effect, indicating that this predominantly originates in the solar wind driver of the ring current as given by VB_s. Again, it is evident that the intensities of the major storms tend to be underestimated compared to observations.

The main factor controlling VB_s is B_s since the solar wind speeds associated with typical streams only range over a factor of $\sim$ 2 (say from $\sim$ 400 to $\sim$ 800 km/s) whereas B_s has a larger range of values. Figure 12 shows the maximum southward field in the solar wind structure that drives the Dst index to minimum values, plotted versus peak Dst for our sample of CIR/stream-associated storms ($cc = 0.586$). Though major storms are associated with larger than average values of B_s ($\sim$ 9 – 19 nT), there are also CIRs with intervals of relatively strong B_s that produce weaker than expected storms since, as discussed above, the storm size also depends on the time variation in the north-south magnetic field component. To provide a comparison with ICME-related storms, we have overplotted in Figure 12 (dashed line) the *Richardson and Cane* [2005] result of fitting peak storm (Dst) size to B_s for a sample of $\sim$ 200 ICME-related storms, $Dst = 8.49B_s + 5.6$ nT. Overall, the dependence between Dst and B_s is similar for both CIR and ICME storms but, for a given B_s, ICMEs are typically more geoeffective by $Dst \sim -30$ nT. A possible reason is that the intervals of southward fields are typically more prolonged in ICMEs, in particular in the case of magnetic clouds that give rise to the majority of larger storms, than in CIRs. The *Richardson and Cane* [2005] $Dst - B_s$ relationship for ICMEs, if applicable to CIRs, suggests that since B_s in CIRs rarely exceeds ~ 20 nT, CIR-generated storms may only be expected to reach $Dst \sim -175$ nT.

Another limit on CIR-associated storm sizes may be based on the OM equations. Minimum Dst^* occurs when

$$\frac{d}{dt}Dst^* = 0, \tag{4}$$

and hence,

$$Q\tau = Dst^*. \tag{5}$$

For maximum observed values of B_s (~ 20 nT), and assuming a typical solar wind speed of say $V \sim 450$ km/s, transverse electric fields reaching ~ -9 mV/m are expected to be associated with CIRs (cp., Table 1), which then imply similar limiting minimum values of $Dst \sim -180$ nT if the storm is allowed to proceed until loss driving and loss terms balance. A caveat is that as discussed above in relation to Figure 11, the OM equations underestimate the size of CIR-associated storms by ~ 20 nT, so the predicted limit may also need to be reduced by a similar amount, to $Dst \sim -200$ nT. The upper values of $B_s \sim 20$ nT found in CIRs presumably result from the maximum field strengths that can typically be achieved from compressing the interplanetary magnetic field by the stream-stream interaction process, and the degree to which these fields, which on average are expected to lie near the ecliptic, are deflected southward. ICMEs can generate stronger storms because their magnetic fields are imposed during CME formation near the Sun and can include configurations (such as flux ropes in the case of magnetic clouds) that may lead to extended intervals of enhanced out-of-the-ecliptic field components. Interaction between fast ICMEs and the upstream solar wind can also lead to compressions and deflections of the sheath magnetic fields that can be highly geoeffective.

While this anticipated limit on the size of CIR-associated storms is consistent with observations in 1996 – 2004, we have also examined whether it holds for an additional 23 probable CIR/stream-associated $Dst \leq -100$ nT storms we have identified between 1972 and 1995. These are listed in Table 2 and plotted in Figure 8. The availability of in-situ plasma and field data is also noted. Where such data were unavailable, to infer the presence of corotating streams we have referred to other observations, such as recurrent geomagnetic activity enhancements and recurrent cosmic ray depressions observed by neutron monitors and the Goddard energetic particle instrument on IMP 8 [e.g., *Richardson et al.*, 1999]. The strongest such storm (September 13, 1999) reached $Dst = -161$ nT, though with the caveat that the "pure" CIR character cannot be confirmed in the absence of in-situ observations. Thus, these additional storms also lie within the expected limit.

Returning to our sample of CIR-associated events in 1966 – 2004, Figure 13 shows that the storm size is poorly correlated with the peak solar wind speed in a stream ($cc = 0.321$) or the change in speed at the stream leading edge ($cc = 0.249$), a reason being that there is essentially no correlation (Figure 14) between B_s in the region that drives the storm and the peak stream speed ($cc = 0.189$). In particular, major storms are not necessarily associated with exceptionally fast streams. The correlations are not significantly improved by considering streams with seasonally favored and unfavored field directions separately.

An intriguing feature of the nine major storms in Table 1 is that four (44%) occurred over a period of less than three solar rotations in September – November, 2002. There was also a CIR-associated storm of $Dst = -98$ nT on October 24 that nearly meets the criteria for inclusion in Table 1. During this period, both CIR- and ICME-associated storms were present. Although, as noted above, the CIR storm on October 7 occurred during the decay of an intense ICME-associated storm, preceding activity does not appear to be a factor in the other major CIR-associated storms. A unique characteristic of the September – November 2002 period is that it coincides with the highest mean values of the IMF intensity and mean solar magnetic field during cycle 23. Figure 8 shows the solar cycle variations in Carrington rotation averages of the mean IMF intensity and the RMS value of daily measurements of the mean solar field from the Wilcox Observatory. The vertical line indicates the time of maximum mean IMF in cycle 23. Although an interesting possibility is that the high mean IMF, which apparently reflects the strong solar fields, contributes to the overall geoeffectiveness of CIRs and streams during late 2002, this cannot be the dominant controlling factor since major CIR storms, such as October 23, 1996, can also occur when the mean IMF is much weaker. In addition, the highest mean fields in late 2002 are also only $<\sim 1$ nT higher than typical mean fields of $\sim 7 - 8$ nT during much of cycle 23, and it seems unlikely that such a small difference alone could account for the strong clustering of major storms at this time. The highest mean IMF intensities (and associated elevated solar mean fields) during the previous two solar cycles are also indicated in Figure 8. Although there is a cluster of 3 major storms around this time in cycle 22, overall the distribution of events in both cycles 22 and 21 is not strongly ordered by these field strengths, with the majority of such storms occurring as the fields decline during the descending phase of each cycle.

Considering all the $Dst \leq -100$ nT storms in 1972 – 2004, they display a clear seasonal effect, illustrated in Figure 15 where the number of storms per calendar month is given for cases where the field in the storm driver is directed away from or towards the Sun. The clear dominance of major storms driven by Sunward- (outward-) directed fields near the spring (autumn) equinox is consistent with the seasonal dependence of CIR-associated geomagnetic activity found above in cycle 23. We also note that *McAllister and Crooker* [1997] reported a seasonal effect in CIR-associated activity during cycle 22.

4. Summary and Conclusions

From the point of view of forecasting major storms, what is the importance of CIR-associated events? First of all, observations suggest that only a few percent of CIRs ($\sim 6\%$ in cycle 23) produce storms that exceed the $Dst = -100$ nT threshold. Based on solar wind parameters associated with CIRs and the OM equations, we estimate that the upper limit on CIR-associated storms is likely to be $Dst \sim -180$ nT. Thus, CIRs are unlikely to be a source of severe storms, at least as measured by Dst, that far exceed this limit. Observations since 1972 are consistent with this expectation. The size of CIR-associated storms can be estimated with limited (~ 1 hour) lead time using upstream real-time plasma/field data and the OM equations, though we note that these equations tend to underestimate the size of major storms by ~ 20 nT. The seasonal effect clearly enhances the geoeffectiveness of CIRs near the equinoxes if the IMF direction is favorable and is an important factor in generating storms with $Dst \leq -100$ nT. Although stream speeds can be predicted fairly successfully from a potential field model, for example [e.g., *Arge and Pizzo*, 2000; *Arge et al.*, 2003], unfortunately they are poor predictors of the geoeffectiveness of streams/CIRs. The source coronal holes in Figure 6 show no unusual configuration in common that might be indicative of a particularly geoeffective stream except that they lie at low latitudes and are frequently equatorward extensions of polar coronal holes that reach low latitudes. Since the magnetic field direction in coronal holes, and hence in the associated streams, can be inferred from solar magnetograms and from knowledge of the solar polar field directions, it should be possible to forecast when CIRs with "favored" IMF configurations will be present near the Earth near the equinoxes, with a potential for generating major storms. On the other hand (though there are no clear examples among the major events discussed in this paper), the most geoeffective structure might also precede the heliospheric current sheet crossing ahead of a stream, in which case, the field direction will be opposite to that in the fast stream.

Major CIR storms appear to avoid solar maximum, are most prevalent during the declining phase of the cycle, and intriguingly may occur preferentially in association with intervals of enhanced IMF intensity, and mean solar magnetic fields. The tendency for events to cluster over several solar rotations also suggests that the best predictor of an upcoming CIR-associated major storm may be the occurrence of such a storm on a preceding solar rotation. It is also important to remember that Dst is only one aspect of the magnetospheric phenomena associated with geomagnetic storms. CIRs are known, for example, to have a greater influence on the strength of the outer radiation belts than CME-driven storms [e.g., *Paulikas and Blake*, 1976; *Lam*, 2004; *Miyoshi and Kataoka*, 2005].

Finally we note that one of the arguments of *McAllister and Crooker* [1997] that CMEs play a role in CIR-associated storms is that "it is generally accepted that major storms cannot be generated by CIRs alone [*Gosling*, 1993; *Tsurutani et al.*, 1995b]. Therefore, the presence of major storms (peak $Dst \leq -100$ nT) at the leading edges of both [seasonally] favored and unfavored sectors also suggests the presence of transients." We conclude, however, that CIRs alone do occasionally produce storms that exceed this level, at least in favored sectors. We also note that CIRs evidently have a rich diversity of field configurations, and searching for the drivers of major CIR-associated storms will almost inevitably lead to the few CIRs that include regions of extended, enhanced southward fields resembling those found in geoeffective transients, even if transients are not involved in these storms.

Acknowledgments. We thank the organizers of the "Living With a Star" CDAW at the George Mason University, Virginia, for the opportunity to meet and discuss these storms, and the members of Working Group 1 for their participation in identifying and interpreting the solar and interplanetary observations. The CDAW website is http://cdaw.gsfc.nasa.gov/geomag_cdaw/. We acknowledge the use of ACE data, available from the ACE Science Center (http://www.srl.caltech.edu/ACE/ASC/), and Genesis data, available at http://genesis.lanl.gov/. WIND data were obtained from the WIND/MFI site (http://lepmfi.gsfc.nasa.gov/) and from the University of Berkeley (http://sprg.ssl.berkeley.edu/wind3dp/). Data from the National Space Science Data Center and National Geophysical Data Center were also used. Wilcox Observatory data are available at http://quake.stanford.edu/~wso/. We also thank R. McPherron for helpful discussions regarding the OM equations, and the referees for their constructive comments.

References

Arge, C. N., and V. J. Pizzo, Improvement in the prediction of solar wind conditions using near-real time solar magnetic field updates, *J. Geophys. Res., 105*, 10465, 2000.

Arge, C. N., D. Odstrcil, V. J. Pizzo, and L. R. Mayer, Improved method for specifying solar wind speed near the Sun, in *Solar Wind Ten*, AIP Conf. Proc. CP679, eds. M. Velli, R. Bruno, and F. Malara, 190, 2003.

Bavassano, B., R. Woo, and R. Bruno, Heliospheric plasma sheet and coronal streamers, *Geophys. Res. Lett., 24*, 1655, 1997.

Belcher, J. W., and L. Davis, Large amplitude Alfvén waves in the interplanetary medium, 2, *J. Geophys. Res., 76*, 3534, 1971.

Burlaga, L. F., Interplanetary stream interfaces, *J. Geophys. Res., 79*, 3717, 1974.

Burlaga, L. F., and R. P. Lepping, The causes of recurrent geomagnetic storms, *Planet. Space Sci., 25*, 1151, 1977.

Cane, H. V., and I. G. Richardson, What caused the large geomagnetic storm of November 1978?, *J. Geophys. Res., 102*, 17, 445, 1997.

Cane, H. V., and I. G. Richardson, Interplanetary coronal mass ejections in the near-earth solar wind during 1996-2002, *J. Geophys. Res., 108(4)*, 10.1029/2002JA009817, 2003.

Cliver, E. W., Y. Kamide, and A. G. Ling, Mountains versus valleys: Semiannual variation of geomagnetic activity, *J. Geophys. Res., 105*, 2413, 2000.

Crooker, N. U., Solar and heliospheric geomagnetic disturbances, *J. Atmosph. Solar Terr. Phys., 62*, 1071, 2000.

Crooker, N. U., and E. W. Cliver, Postmodern view of M-regions, *J. Geophys. Res., 99*, 23,383, 1994.

Crooker, N. U., C.-L. Huang, S. M. Lamassa, D. E. Larson, S. W. Kahler, and H. E. Spence, Heliospheric plasma sheets, *J. Geophys. Res., 109*, doi:10.1029/2003JA010170, 2004a.

Crooker, N. U., S. W. Kahler, D. E. Larson, and R. P. Lin, Large-scale magnetic field inversions at sector boundaries, *J. Geophys. Res., 109*, doi:10.1029/2003JA010278, 2004b

Dungey, J. W., Interplanetary magnetic field and the auroral zones, *Phys. Rev. Lett., 6*, 47, 1961.

Fenrich, F. R., and J. G. Luhmann, Geomagnetic response to magnetic clouds of different polarity, *Geophys. Res. Lett., 25*, 2999, 1998.

Forsyth, R. J., and E. Marsch, Solar origin and interplanetary evolution of stream interfaces, *Space Sci. Rev., 89*, 7, 1999.

Gonzalez, W. D., B. T. Tsurutani, and A. L. Clúa de Gonzalez, Interplanetary origin of geomagnetic storms, *Space Sci. Rev., 88*, 529, 1999.

Gosling, J. T., Coronal mass ejections and magnetic flux ropes in interplanetary space, in *Physics of Magnetic Flux Ropes*, Geophys. Monogr. Ser., vol. 58, eds. C. T. Russell, E. R. Priest, and L. C. Lee, p. 343, AGU, Washington, D. C., 1990.

Gosling, J. T., The solar flare myth, *J. Geophys. Res., 98*, 18,937, 1993.

Gosling, J. T., J. R. Asbridge, S. J. Bame, and W. C. Feldman, Solar Wind Stream Interfaces, *J. Geophys. Res., 83*, 1401, 1978.

Gosling, J. T., D. J. McComas, J. L. Phillips, and S. J. Bame, Geomagnetic activity associated with Earth passage of interplanetary shock disturbances and coronal mass ejections, *J. Geophys. Res., 96*, 7831, 1991.

Klein, L. W., and L. F. Burlaga, Interplanetary magnetic clouds at 1 AU, *J. Geophys. Res., 87*, 613, 1982.

Kahler, S. W., and R. P. Lin, An examination of directional discontinuities and magnetic polarity changes around interplanetary sector boundaries using $E > 2$ keV electrons, *Solar Phys., 161*, 183, 1995.

Lam, H.-L., On the prediction of relativistic electron fluence based on its relationship with geomagnetic activity over a solar cycle, *J. Atmos. Solar-Terr. Phys., 66*, 1703, 2004.

Lepping, R. P., C. C. Wu, and D. Berdichevsky, Automatic identification of magnetic clouds and cloud-like regions at 1 AU: Occurrence rate and other properties, *Ann. Geophysicae*, in press, 2005.

Lepri, S. T., T. H. Zurbuchen, L. A. Fisk, I. G. Richardson, H. V. Cane, and G. Gloeckler, Iron charge distribution as an identifier of interplanetary coronal mass ejections, *J. Geophys. Res., 106*, 29,231, 2001.

McAllister, A. H., and N. U. Crooker, Coronal mass ejections, corotating interaction regions, and geomagnetic storms, in "Coronal Mass Ejections", eds. N. U. Crooker, J. A. Joselyn, and J. Feynman, A.G.U. Geophysical Monogr. 99, 279, 1997.

McAllister, A. H., D. J. Knipp, N. U. Crooker, T. Mukai, and S. Kokubun, Identification of solar drivers: The November 3–4, 1993, geomagnetic storm, *J. Geophys. Res., 103*, 26221, 1998.

Miyoshi, Y., and R. Kataoka, Ring current ions and radiation belt electrons during geomagnetic storms driven by coronal mass ejections and corotating interaction regions, *Geophys. Res. Lett.*, doi:10.1029/2005GL024590, in press, 2005.

Neugebauer, M., J. T. Steinberg, R. L. Tokar, B. L. Barraclough, E. E. Dors, R. C. Wiens, D. E. Gingerich, D. Luckey, and D. B. Whiteaker, Genesis on-board determination of the solar wind flow regime, *Space Sci. Rev., 105*, 661, 2003.

O'Brien, T., and R. McPherron, An empirical phase space analysis of ring current dynamics: Solar wind control of injection and decay, *J. Geophys. Res., 105*, 7707, 2000.

Paulikas, G. A., and J. B. Blake, Modulation of trapped energetic electrons at 6.6 Re by the interplanetary magnetic field, *Geophys. Res. Lett., 3*, 277, 1976.

Perreault, P., and S.-I. Akasofu. A study of geomagnetic storms, *Geophys. J. R. Astr. Soc., 54*, 547, 1978.

Richardson, I. G., and H. V. Cane, Regions of abnormally low proton temperature in the solar wind (1965-1991) and their association with ejecta, *J. Geophys. Res., 100*, 23,397, 1995.

Richardson, I. G., and H. V. Cane, Identification of interplanetary coronal mass ejections at 1 AU using multiple solar wind plasma composition anomalies, *J. Geophys. Res., 109*, doi:10.1029/2004JA010598, 2004.

Richardson, I. G., and H. V. Cane, A survey of interplanetary coronal mass ejections in the near-Earth solar wind during 1996 – 2005, in *Solar Wind 11*, in press, 2005.

Richardson, I. G., H. V. Cane, and E. W. Cliver, Sources of geomagnetic storms for solar minimum and maximum conditions during 1972 – 2000, *Geophys. Res. Lett., 28*, 2569, 2001.

Richardson, I. G., H. V. Cane, and G. Wibberenz, A 22-year dependence in the size of near-ecliptic corotating cosmic ray depressions during five solar minima, *J. Geophys. Res., 104*, 12,549, 1999.

Russell, C. T., and R. L. McPherron, Semiannual variation of geomagnetic activity, *J. Geophys. Res., 78*, 92-108, 1973.

Schwenn, R., Large-scale structure of the interplanetary medium, in R. Schwenn and E. Marsch(eds.), *Physics of the Inner Heliosphere*, Vol. 1, p. 99, Springer-Verlag, Berlin, Heidelberg, New York, 1990.

Smith, E. J., A. Balogh, M. Neugebauer, and D. McComas, Ulysses observations of Alfvén waves in the southern and northern solar hemispheres, *Geophys Res. Lett., 22*, 3381, 1995.

Tsurutani, B. T., and W. D. Gonzalez, The interplanetary causes of magnetic storms: A review, in B. T. Tsurutani, W. D. Gonzalez, Y. Kamide, and J. K. Arballo (eds.), *Magnetic Storms*, Geophys. Monogr., 98, AGU, Washington, D.C., p. 77, 1997.

Tsurutani, B. T., C. M. Ho, J. K. Araballo, B. E. Goldstein, and A. Balogh, Large amplitude IMF fluctuations in corotating interaction regions: Ulysses at midlatitudes, *Geophys. Res. Lett., 22*, 3397, 1995a.

Tsurutani, B. T., W. D. Gonzalez, A. L. C. Gonzalez, and F. Tang, Interplanetary origin of geomagnetic activity in the declining phase of the solar cycle, *J. Geophys. Res., 100*, 21,717, 1995b.

Watari, S., The effect of the high-speed stream following the corotating interaction region on the geomagnetic activities, *Ann. Geophysicae, 15*, 622, 1997.

Wimmer-Schweingruber, R. F., R. von Steiger, and R. Paerli, Solar Wind Stream Interfaces in Corotating Interaction Regions: SWICS/Ulysses Results, *J. Geophys. Res., 102*, 17,407, 1997.

Winterhalter, D., E. J. Smith, M. E. Burton, N. Murphy, and D. J. McComas, The heliospheric plasma sheet, *J. Geophys. Res., 99*, 6667, 1994.

Zhang, J., K. P. Dere, R. A. Howard, and V. Bothmer, Identification of the solar sources of major geomagnetic storms between 1996 and 2000, *Astrophys. J., 582*, 520, 2003.

Zhao, X., Interaction of fast steady flow with slow transient flow: A new cause of shock pair and interplanetary B_z event, *J. Geophys. Res, 97*, 15,051, 1992.

D. B. Berdichevsky, R. Kataoka, and B. J. Thompson, Code 612, NASA Goddard Space Flight Center, Greenbelt, MD, 20771 (dberdich@pop600.gsfc.nasa.gov; ryuho@nict.go.jp; Barbara.j.thompson@nasa.gov); D. A. Biesecker, NOAA/SEC W/NP9, 325 Broadway, Boulder, CO 80305 (doug.biesecker@noaa.gov); J. C. Kasper, MIT Center for Space Research, 37-673 77 Massachusetts Avenue, Cambridge, MA 02139 (jck@mit.edu); I. G. Richardson, Code 661, NASA Goddard Space Flight Center, Greenbelt, MD, 20771 (richardson@lheavx.gsfc.nasa.gov); J. T. Steinberg, MS D466, Los Alamos National Laboratory, Los Alamos, NM 87545 (jsteinberg@lanl.gov); D. W. Webb, Boston College, Inst. for Scientific Research, Chestnut Hill, MA 02467 (David.Webb.ctr@hanscom.af.mil); C.-C. Wu, CSPAR/University of Alabama in Huntsville, Code 696, NASA Goddard Space Flight Center, Greenbelt, MD, 20771(wuc@cspar.uah.edu); J. Zhang, George Mason University, 4400 University Dr., Fairfax, VA 22030 (jiez@scs.gmu.edu); A. N. Zhukov, Royal Observatory of Belgium, Avenue Circulaire 3, B-1180 Brussels, Belgium (Andrei.Zhukov@oma.be)

Figure 1. Three CIR-associated $Dst \leq -100$ nT storms driven by structures (several hour duration intervals of persistent southward field) in decelerated fast solar wind following the stream interface (indicated by green vertical lines). The red vertical line in the bottom panel indicates passage of a reverse shock.

Figure 2. Three major storms driven by structures ahead of the stream interface.

Figure 3. Two major storms driven by southward field structures prior to and following the stream interface. Forward and reverse shocks are indicated by red vertical lines on November 20, 2002 and July 12, 2003, respectively.

Figure 4. A major storm driven by an interaction region between two high-speed streams. The red vertical line indicates a reverse shock.

Figure 5. North-south (z) components of the solar wind magnetic field and velocity in the vicinity of the interplanetary structures (several hour duration regions of persistent southward fields (-ve B_z)) that drive the geomagnetic storms in Table 1. The pervasive correlated variations between B_z and V_z are indicative of Alfvén waves.

Figure 6. SOHO EIT Fe XV observations of the coronal hole sources for the high-speed streams associated with the storms in Table 1.

Figure 7. A well-developed CIR including southward magnetic fields of more than 20 nT that gives rise to only a modest storm because of the large both positive and negative fluctuations in B_z due to Alfvén waves. In addition, the high plasma densities in the heliospheric plasma sheet drive Dst temporarily positive.

Table 1. CIR-Associated $Dst \leq -100$ nT Storms in 1996 – 2004

Storm Peak (UT)	$Dst(Dst^*)$ (nT)	B_s[a] (nT)	B Direction[b]	E_y[c] (mV/m)	V_{slow}[d] (km/s)	V_{fast}[e] (km/s)	dV[f] (km/s)	Driver Location [g]	HCS?[h]	Notes
1996										
Oct. 23, 03	-105 (-105)	12	+	-7	450	670	220	F'	N	Also *Zhang et al.* [1996]
1997										
No Events										
1998										
Mar. 10, 21	-116 (-119)	17	–	-9	300	600	300	F'	Y	
1999 – 2001										
No Events										
2002										
Sept. 4, 06	-109 (-110)	20	+	-7	350	500	150	I/F'	Y	Preceding ICME with $B_z > 0$?
Oct. 7, 08	-115 (–)	10	+	-3	400	500	100	S'	N	Preceding storm
Oct. 14, 14	-100 (-104)	16	+	-5	280	580	300	S'	Y	
Nov. 21, 11	-128 (-133)	16	+	-10	380	740	360	S'+F'	Y	Preceding "flux rope" with $B_z > 0$?
2003										
Jul. 12, 06	-118 (-120)	15	+	-9	350	700	350	S'+F'	Y	ICME-driven 1st component
Jul. 16, 13	-117 (-122)	12	–	-6	550	690	140	S'	N	In high-speed stream
2004										
Feb. 11, 18	-109 (-116)	15	–	-6	380	700	320	S'	Y	

[a] Maximum southward magnetic field (nT).
[b] Magnetic field direction in structure driving storm: + = outward; – = sunward.
[c] Solar wind electric field y-component.
[d] Solar wind speed in slow solar wind preceding CIR.
[e] Solar wind speed in fast solar wind following CIR
[f] Change in solar wind speed.
[g] S'=accelerated slow solar wind ahead of stream interface; F'=decelerated fast solar wind following stream interface; I=stream interface.
[h] Heliospheric current sheet (sector boundary) encountered in vicinity of CIR?

Table 2. "CIR-Associated" $Dst \leq -100$ nT Storms in 1972 – 1995

Date (UT)	*Dst* (nT)	Magnetic Field	Plasma	B Direction	Notes
1973 Feb 21	-121	Yes	Yes	−	
1975 Nov 9	-110	No	Partial	...	
1977 Dec 11	-112	Yes	Yes	+	
1983 Mar 12	-132	No	No	...	
1984 Mar 28	-105	Partial	Partial	−	
1984 Aug 1	-112	Partial	Partial	+	
1986 Oct 13	-101	Partial	No	...	
1989 Apr 26	-132	Yes	Yes	−	
1991 Aug 2	-114	Yes	Yes	+	
1991 Aug 30	-107	Yes	Yes	+	
1991 Nov 22	-139	Partial	Partial	+	
1992 Sep 17	-140	No	No	...	
1992 Sep 29	-118	No	No	...	
1993 Mar 9	-137	Yes	Yes	−	
1993 Sep 13	-161	No	No	...	
1993 Nov 4	-119	No	Partial	...	
1993 Dec 3	-117	Yes	Yes	+	
1994 Feb 6	-126	Partial	Partial	+	Also *Watari* [1997]
1994 Mar 7	-109	Yes	Yes	−	Also *Watari* [1997]
1994 Apr 4	-111	No	No	...	Also *Watari* [1997]
1994 Nov 26	-117	Yes	Yes	+	
1995 Mar 26	-107	Yes	Yes	−	
1995 Apr 7	-149	Yes	Yes	−	

Figure 8. Minimum *Dst* in CIRs during 1972 – mid-2005 (events with $Dst \leq -100$ nT only are shown prior to 1996) plotted together with the mean interplanetary magnetic field strength at Earth (solar rotation averages) and the solar mean magnetic field strength (specifically solar rotation root mean squares of daily values) measured at the Wilcox observatory. Vertical lines indicate times of maximum mean interplanetary field in solar cycles 21 – 23.

Figure 9. Histogram of minimum *Dst* values associated with 159 CIRs and 281 ICMEs in 1996 – 2005.

Figure 10. Seasonal variation in CIR-associated geomagnetic activity observed (left) and predicted by the OM equations (right) for cases where the magnetic fields in the activity driver are directed away (top) or towards (bottom) the Sun. Monthly averages are also indicated.

Figure 11. Predicted minimum Dst^* from the OM equations for CIR-associated activity plotted versus observed minimum *Dst* and Dst^*.

Figure 12. Minimum *Dst* vs. maximum B_s in CIRs during 1996 – 2005. For comparison, the dashed line indicates the Dst–B_s relationship inferred for ICMEs by *Richardson and Cane* [2005].

Figure 13. Minimum *Dst* vs. maximum solar wind speed and change in solar wind speed at the stream leading edge for CIRs/streams in 1996 – 2005, showing little correlation between *Dst* and these stream parameters.

Figure 14. Maximum stream speed vs. B_s in the structures driving minimum *Dst* for CIRs/streams in 1996 – 2005.

Figure 15. Number of $Dst \leq -100$ nT storms in Tables 1 and 2 per calendar month, divided into those driven by sunward or anti-solar fields, demonstrating the clear seasonal dependence.

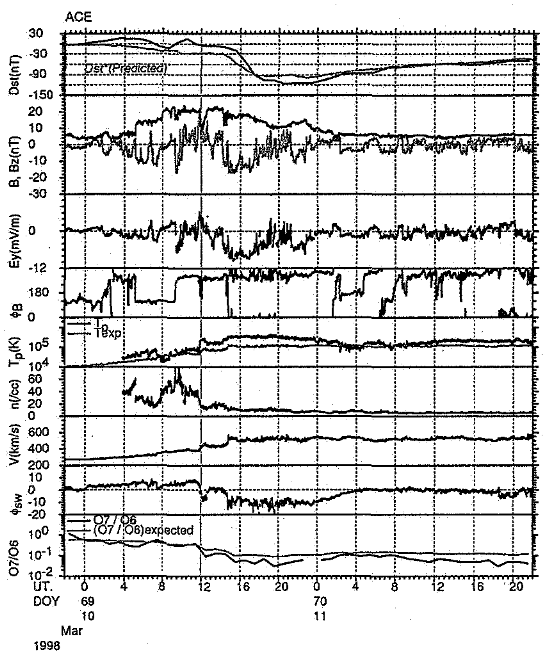
ACE
Dst(nT)
Dst*(Predicted)
B, Bz(nT)
Ey(mV/m)
φB
Tp(K)
Tp
Texp
n(/cc)
V(km/s)
φsw
O7/O6
O7 / O6
(O7 / O6)expected
UT.
DOY 69
10
70
11
Mar
1998

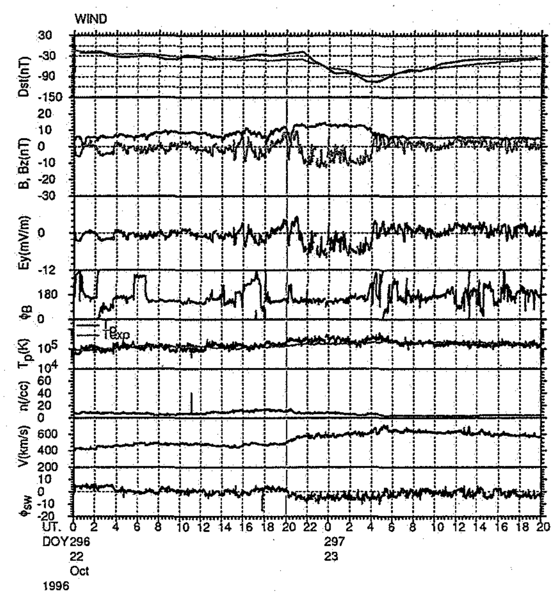
WIND
Dst(nT)
B, Bz(nT)
Ey(mV/m)
φB
Tp(K)
Tp
Texp
n(/cc)
V(km/s)
φsw
UT.
DOY 296
22
297
23
Oct
1996

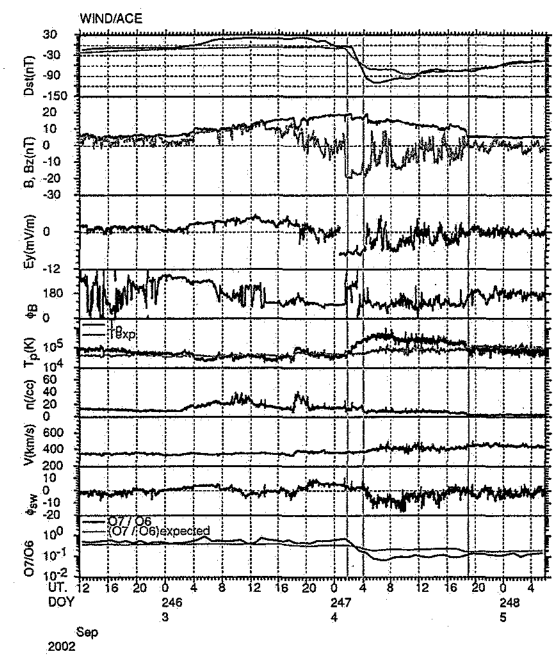
WIND/ACE
Dst(nT)
B, Bz(nT)
Ey(mV/m)
φB
Tp(K)
Tp
Texp
n(/cc)
V(km/s)
φsw
O7/O6
O7 / O6
(O7 / O6)expected
UT.
DOY
246
3
247
4
248
5
Sep
2002

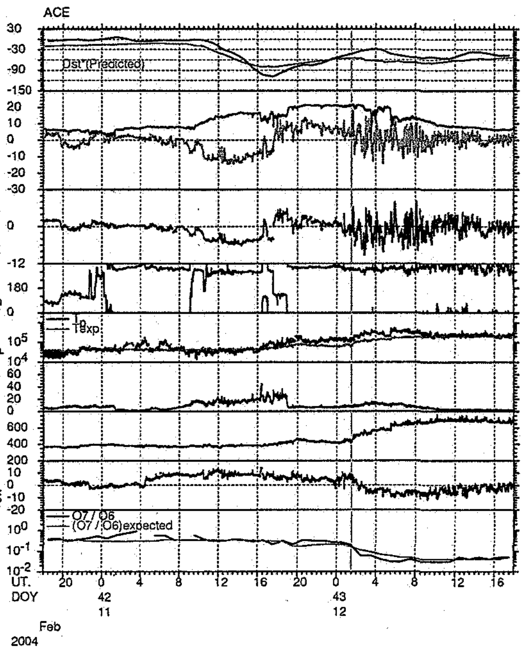
ACE
Dst(nT)
Dst*(Predicted)
B, Bz(nT)
Ey(mV/m)
φB
Tp(K)
Tp
Texp
n(/cc)
V(km/s)
φsw
O7/O6
O7 / O6
(O7 / O6)expected
UT. 20 0 4 8 12 16 20 0 4 8 12 16
DOY 42 43
11 12
Feb
2004

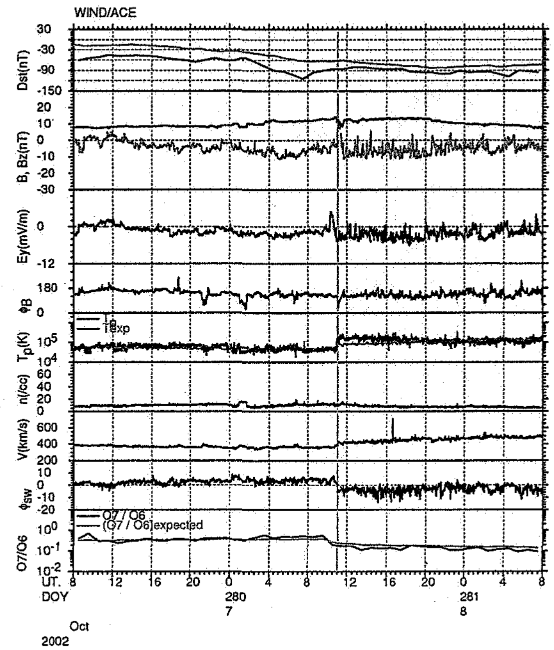
WIND/ACE
Dst(nT)
B, Bz(nT)
Ey(mV/m)
φB
Tp(K)
Tp
Texp
n(/cc)
V(km/s)
φsw
O7/O6
O7 / O6
(O7 / O6)expected
UT. 8 12 16 20 0 4 8 12 16 20 0 4 8
DOY 280 281
7 8
Oct
2002

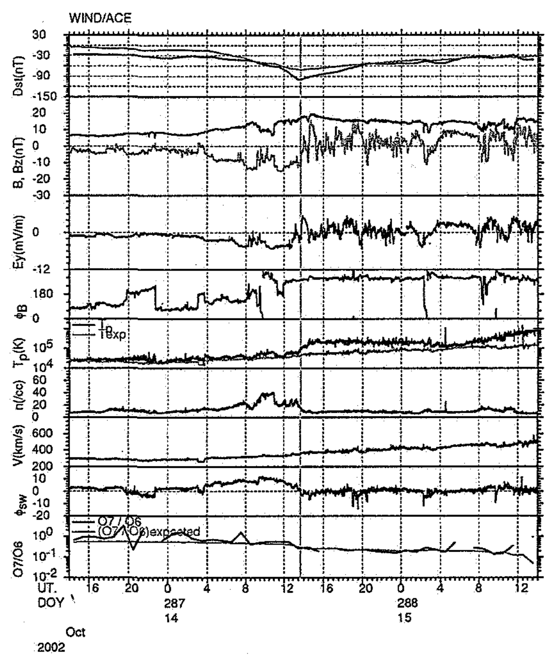
WIND/ACE
Dst(nT)
B, Bz(nT)
Ey(mV/m)
φB
Tp(K)
Tp
Texp
n(/cc)
V(km/s)
φsw
O7/O6
O7 / O6
(O7 / O6)expected
UT. 16 20 0 4 8 12 16 20 0 4 8 12
DOY 287 288
14 15
Oct
2002

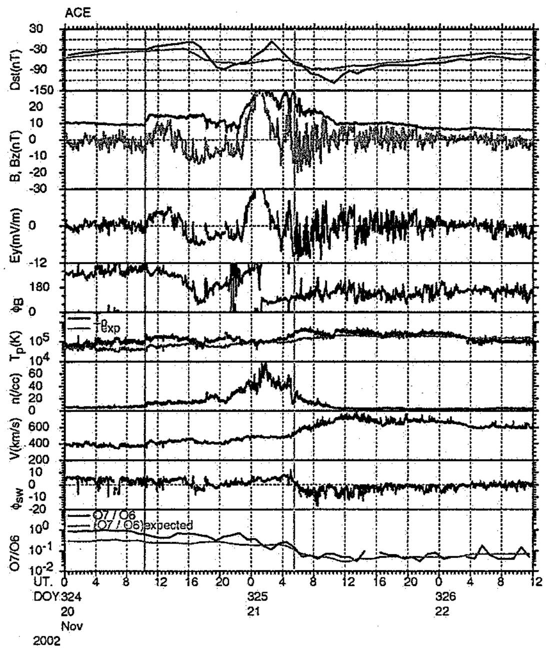

ACE
Dst(nT)
B, Bz(nT)
Ey(mV/m)
φB
Tp(K)
Tp
Texp
n(/cc)
V(km/s)
φsw
O7/O6
O7 / O6
(O7 / O6)expected
UT.
DOY 324
20
Nov
2002
325
21
326
22

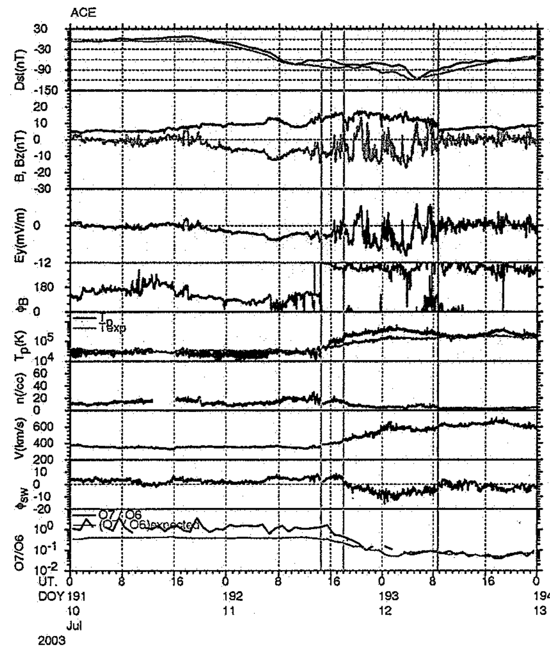

ACE
Dst(nT)
B, Bz(nT)
Ey(mV/m)
φB
Tp(K)
Tp
Texp
n(/cc)
V(km/s)
φsw
O7/O6
O7 / O6
(O7 / O6)expected
UT.
DOY 191
10
Jul
2003
192
11
193
12
194
13

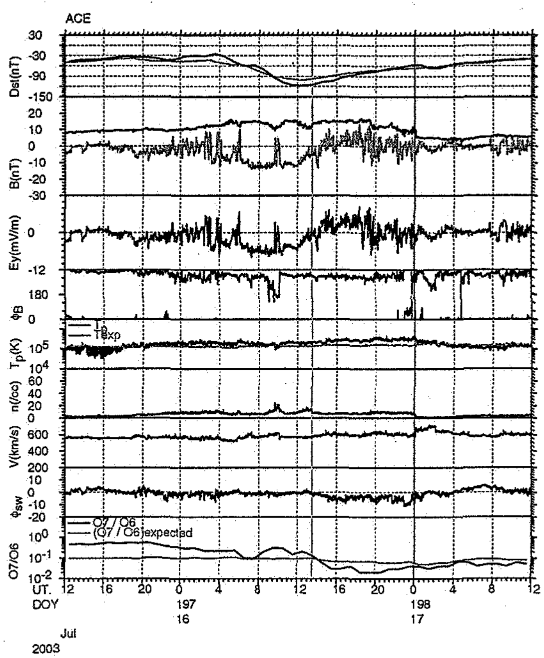

ACE
Dst(nT)
B(nT)
Ey(mV/m)
ϕ_B
Tp(K)
Tp
Texp
n(/cc)
V(km/s)
ϕ_{sw}
O7/O6
O7 / O6
(O7 / O6)expected
UT
DOY
197
16
198
17
Jul
2003

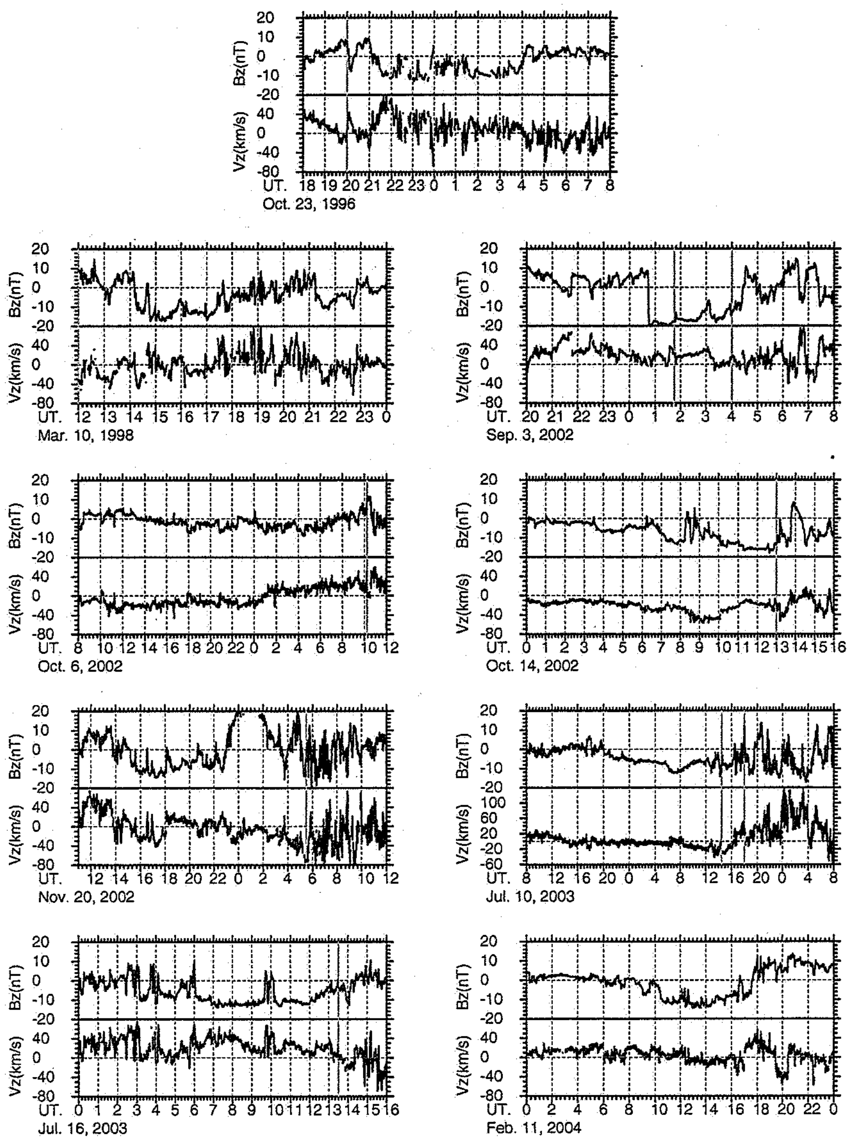
Bz(nT)
Vz(km/s)
UT.
Oct. 23, 1996
Mar. 10, 1998
Sep. 3, 2002
Oct. 6, 2002
Oct. 14, 2002
Nov. 20, 2002
Jul. 10, 2003
Jul. 16, 2003
Feb. 11, 2004

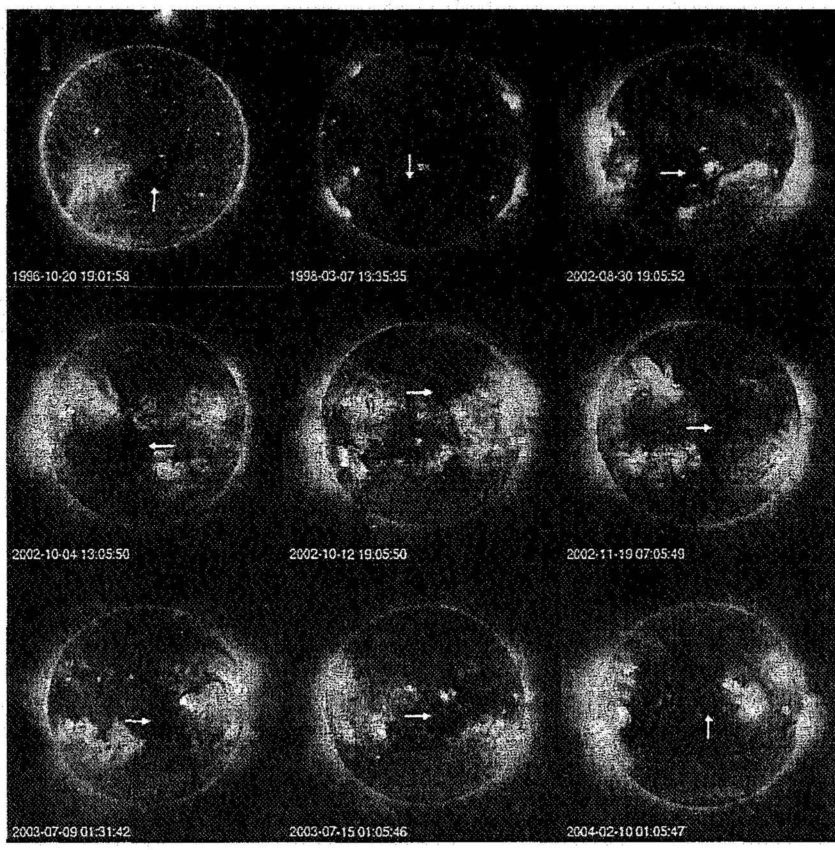
1996-10-20 19:01:58
1998-03-07 13:35:25
2002-08-30 19:05:52
2002-10-04 13:05:50
2002-10-12 19:05:50
2002-11-19 07:05:49
2003-07-09 01:31:42
2003-07-15 01:05:46
2004-02-10 01:05:47

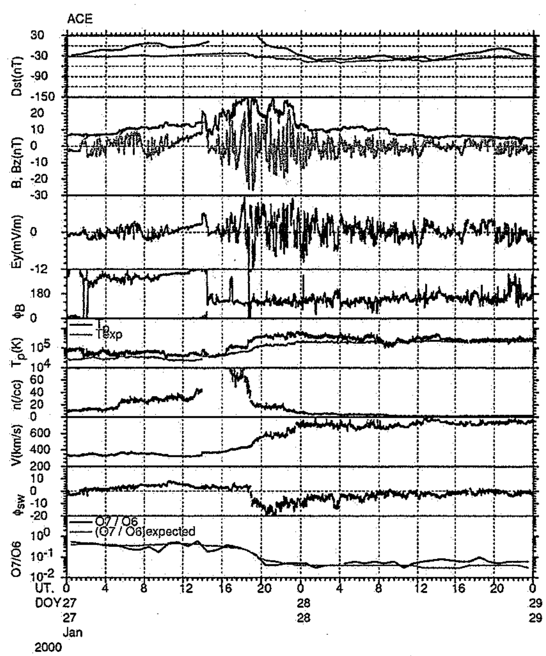

ACE
Dst(nT)
B, Bz(nT)
Ey(mV/m)
φB
Tp(K)
Tp
Texp
n(/cc)
V(km/s)
φsw
O7/O6
O7 / O6
(O7 / O6)expected
UT.
DOY
Jan
2000

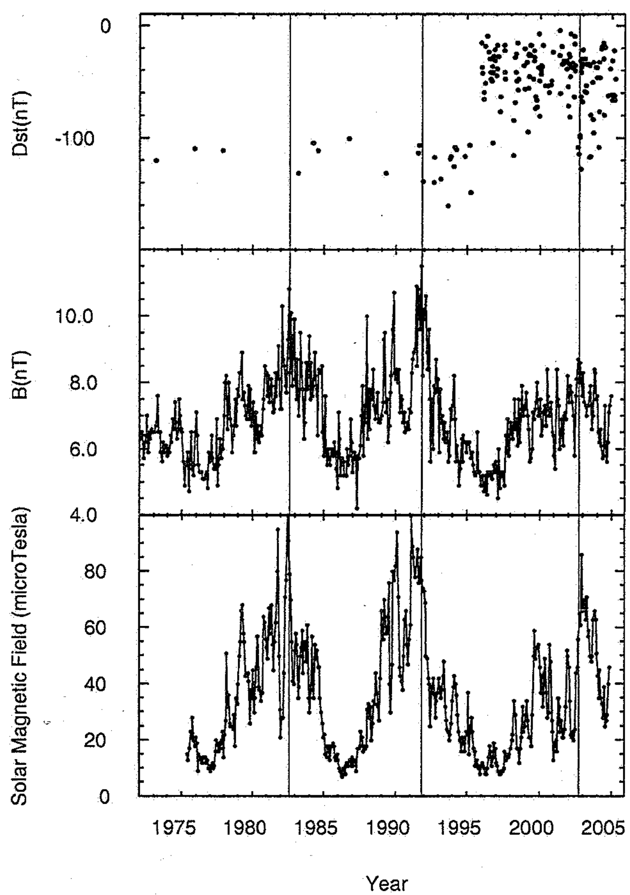

Dst(nT)
0
-100
B(nT)
10.0
8.0
6.0
4.0
Solar Magnetic Field (microTesla)
80
60
40
20
0
1975
1980
1985
1990
1995
2000
2005
Year

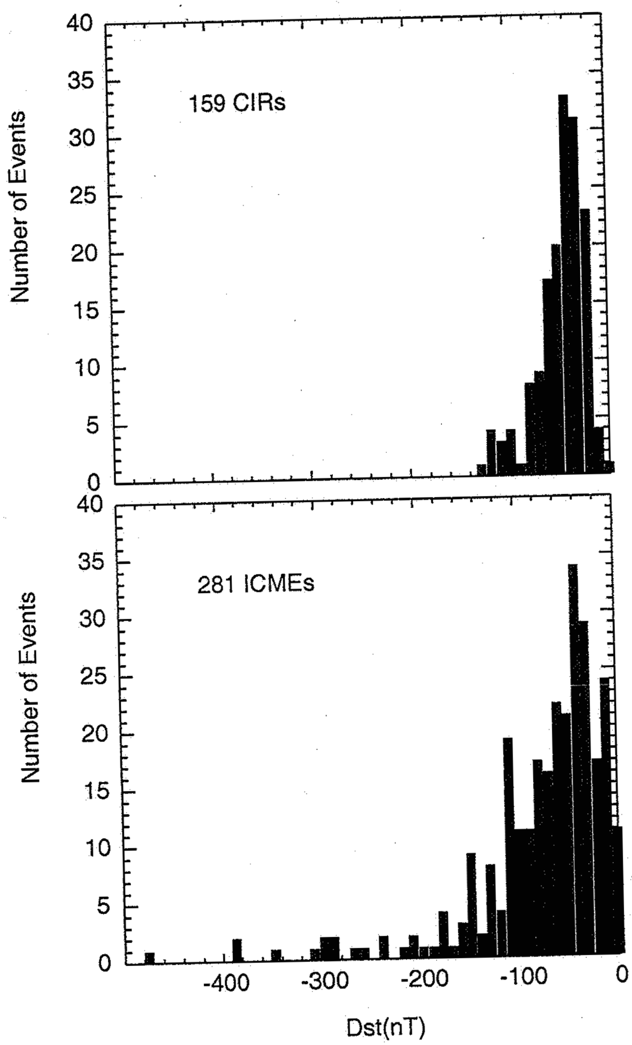

159 CIRs
281 ICMEs
Number of Events
Dst(nT)
40
35
30
25
20
15
10
5
0
-400
-300
-200
-100

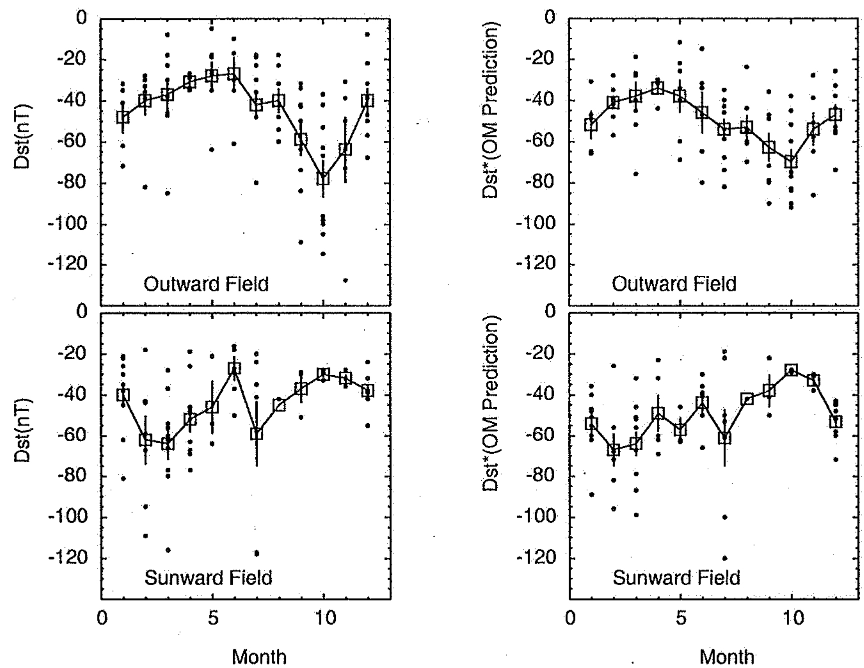

Dst(nT)
Outward Field
Sunward Field
Dst*(OM Prediction)
Month

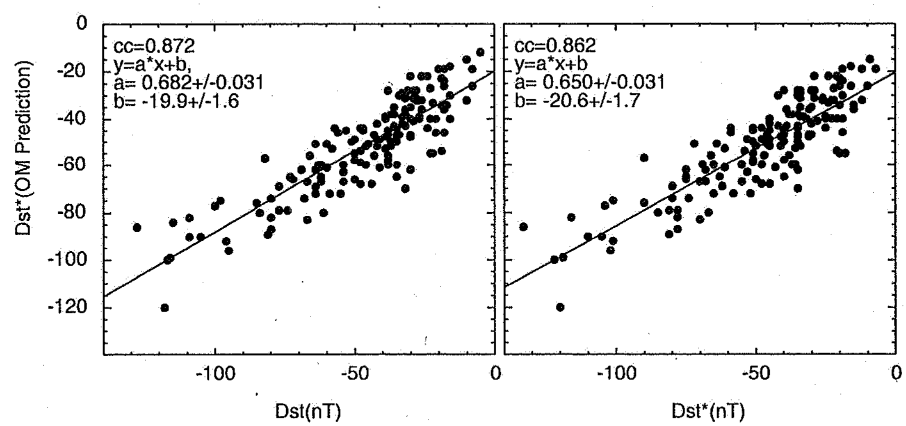
cc=0.872
y=a*x+b,
a= 0.682+/-0.031
b= -19.9+/-1.6
cc=0.862
y=a*x+b
a= 0.650+/-0.031
b= -20.6+/-1.7
Dst*(OM Prediction)
0
-20
-40
-60
-80
-100
-120
-100
-50
0
Dst(nT)
Dst*(nT)

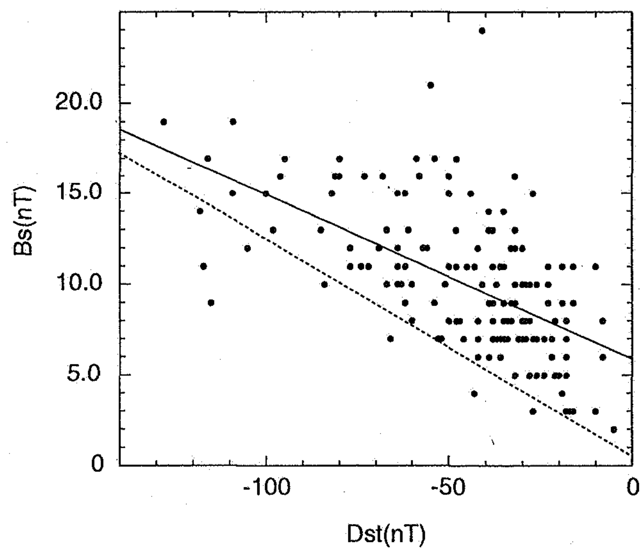
Bs(nT)
20.0
15.0
10.0
5.0
0
-100
-50
0
Dst(nT)

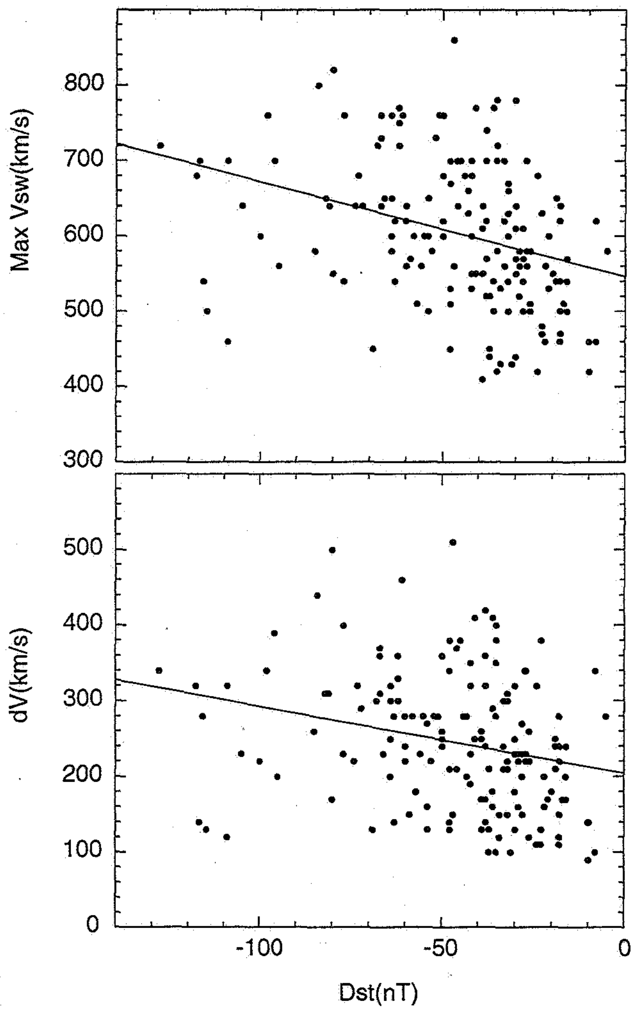

Max Vsw(km/s)
800
700
600
500
400
300
dV(km/s)
500
400
300
200
100
0
-100
-50
0
Dst(nT)

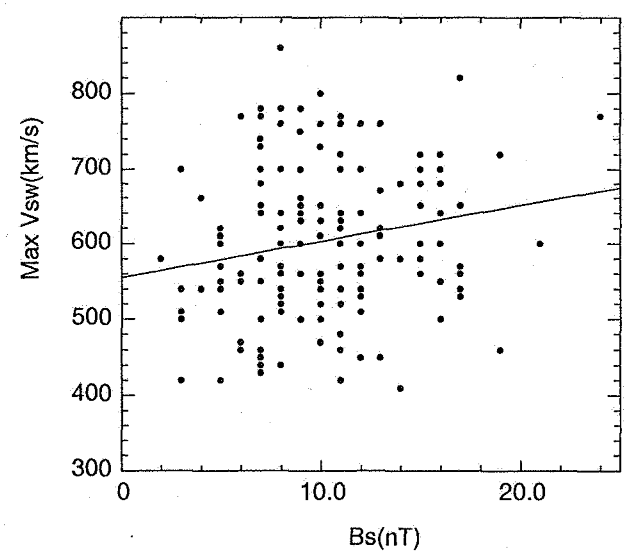

Max Vsw(km/s)
800
700
600
500
400
300
0
10.0
20.0
Bs(nT)

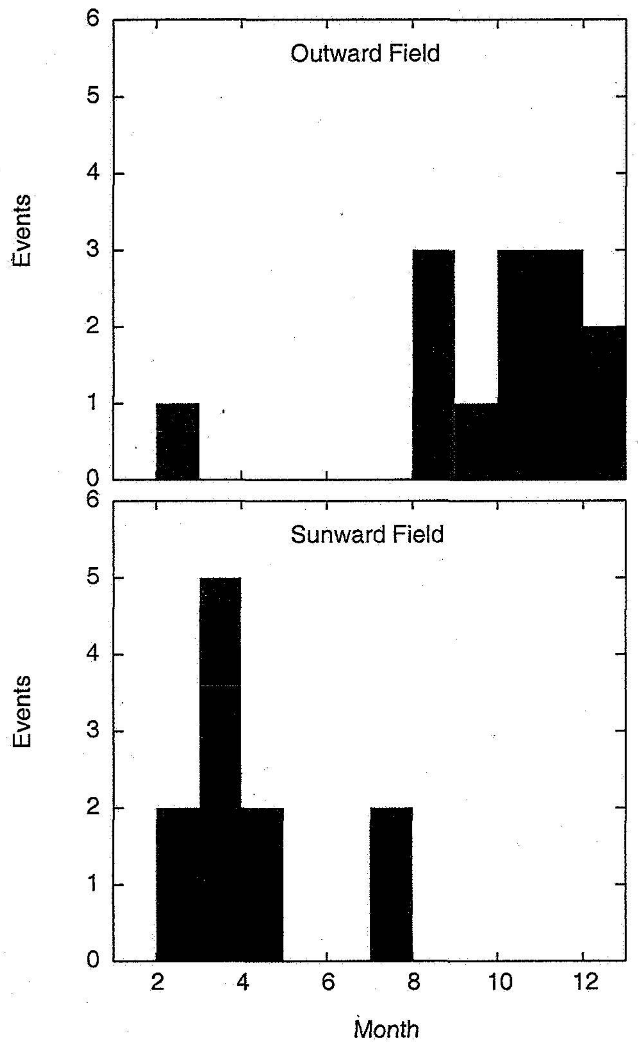

Outward Field
Sunward Field
Events
Events
Month
0
1
2
3
4
5
6
2
4
6
8
10
12